General-Purpose Programmable Photonic Circuit as an Ising Hamiltonian Computing Engine

José Roberto Rausell-Campo*
Photonics Research Lab, iTEAM
Universitat Politècnica de Valencia
Valencia, Spain
joraucam@upv.es

Nayem Al Kayed*
Dept. of Physics, Eng. Physics and Astronomy
Queen's University
Kingston, Canada
nayemal.kayed@queensu.ca

Bhavin Shastri
Dept. of Physics, Eng. Physics and Astronomy
Queen's University
Kingston, Canada
bhavin.shastri@queensu.ca

José Capmany Francoy
Photonics Research Lab, iTEAM
Universitat Politècnica de Valencia
Valencia, Spain
jcapmany@iteam.upv.es

2025 Asia Communications and Photonics Conference (ACP) | 979-8-3503-5740-0/25/$31.00 ©2025 IEEE | DOI: 10.1109/ACP66871.2025.11350411

***Abstract*—Photonic Ising machines exploit the intrinsic parallelism and ultrafast speeds of optical hardware to accelerate ground-state searches for combinatorial optimization. By embedding this functionality into a reconfigurable, general-purpose hexagonal-mesh photonic processor, we obtain a scalable platform capable to address diverse optimization tasks. We present a novel optoelectronic Ising solver in which the programmable photonic chip performs on-chip matrix multiplications to evaluate the Hamiltonian, while an electronic simulated-annealing loop drives iterative spin updates. As a proof of concept, we implement our architecture on the 72-unit-cell SmartLight processor and experimentally solve a three-node ferromagnetic coupling problem with external bias. To our knowledge, this constitutes the first demonstration of an Ising machine on a general-purpose hexagonal photonic mesh, paving the way for integrated photonic accelerators in optical computing and signal processing systems.**

***Index Terms*—programmable photonics, photonic ising machines, photonic integrated circuit**

I. Introduction

Combinatorial optimization problems are found in a wide array of scenarios, including logistics, finance, circuit synthesis and drug discovery [1], [2]. These tasks can be mapped onto an Ising model by encoding each variable as a binary spin $\sigma_i \in \{\pm 1\}$, leading to the Hamiltonian

$$H = \frac{1}{2} \sum_{<i,j>} J_{ij}\, \sigma_i\, \sigma_j \; - \; \sum_i h_i\, \sigma_i \qquad (1)$$

where J_{ij} denotes spin–spin couplings and h_i represents an external bias. Finding the ground state of this Hamiltonian is equivalent to solving the original optimization problem.

This work was supported by the European Research Council (ERC) Advanced Grant program under grant Agreement No. 101097092 (ANBIT), and the COMCUANTICA/005 and COMCUANTICA/006 grants, funded by the European Union through NextGenerationEU (PRTR-C17) with the support of the Spanish Ministry of Science and Innovation and the Generalitat Valenciana. *These authors contributed equally to this work.

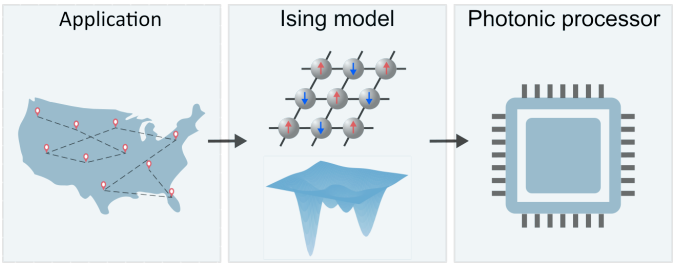

Fig. 1: A schematic of the combinatorial-optimization workflow: a discrete problem is mapped onto an Ising Hamiltonian, and its ground-state solution is found by minimizing the corresponding energy landscape on a photonic processor.

However, the number of possible configurations grows exponentially with the spin count, imposing prohibitive computational and energy requirements on conventional von Neumann processors. This bottleneck, increased by the slowing of Moore's law, has driven the development of specialized, energy-efficient hardware accelerators for large-scale optimization [3], [4].

Ising machines have been realized across diverse hardware platforms, including CMOS-based annealers [5], magnetic tunnel junction arrays [6] and superconducting quantum circuits [7]. Photonic implementations stand out for their intrinsic parallelism, ultrafast operation and low propagation losses [8]. Early versions using bulk optics and fiber loops demonstrated accelerated matrix–vector multiplications [9], but were limited by alignment sensitivity, stability and large footprints. These challenges have motivated the move to integrated photonics. In particular, programmable photonic processors, constructed from reconfigurable meshes of tunable Mach–Zehnder interferometers, offer a compact, robust, on-chip platform for universal linear transformations [10], [11]. An schematic of the workflow of photonic Ising machines is presented in Fig. 1.

In this work, we introduce the first on-chip programmable photonic Ising machine on a general-purpose processor, which combines an eigendecomposition-based Hamiltonian solver with a simulated-annealing algorithm. Spin variables are encoded as optical phase shifts, and following the photonic vector–matrix multiplication by the orthogonal and diagonal matrices resulting from the decomposition of the Ising coupling matrix, the Ising Hamiltonian is recovered via a single on-chip intensity measurement [12]. A digital feedback loop then performs iterative spin updates according to the measured energy and a temperature-dependent acceptance rule [13]. Our proof-of-concept employs the SmartLight processor from iPronics, a hexagonal mesh of thermally tunable MZIs [14], to compute Hamiltonians for coupling matrices up to 4×4. We validate this photonic annealer on a three-node ferromagnetic problem achieving success probabilities approaching unity in most cases. These results lay the groundwork toward fully integrated, programmable photonic architectures for large-scale combinatorial optimization with unprecedented speed and energy efficiency.

II. Architecture and Working Principle

We propose the combination of an eigendecomposition-based Ising solver for Hamiltonian calculation with a simulated annealing algorithm for optimization. The eigendecomposition-based Ising solver is implemented on a hexagonal, reconfigurable photonic mesh to perform the most demanding linear algebra operations in the optical domain.

In the Ising model, the matrix J is symmetric and thus, we can take advantage of the properties of this type of matrices. A symmetric matrix can easily be diagonalized with its eigenbasis such that one can write back J as $J = Q^T \Lambda Q$. Here, Q is an orthogonal matrix whose columns are the eigenvectors of J, and Λ is a diagonal matrix containing the eigenvalues of J. For further simplification, Λ can be decomposed into the multiplication of two diagonal matrices $\Lambda = \sqrt{D}\sqrt{D}$. Then, we get

$$H(\sigma) = -\frac{1}{2}\sigma^T Q^T \sqrt{D}\sqrt{D} Q\sigma = -\frac{1}{2}(\sqrt{D}Q\sigma)^T(\sqrt{D}Q\sigma) \tag{2}$$

It can be shown that if we encode the vector-matrix multiplication $\sqrt{D}Q\sigma$ in the optical domain, a single on-chip intensity measurement then yields the corresponding Hamiltonian value $H(\sigma)$ via direct photo-detection as follows

$$H(\sigma) = \frac{1}{2}\left(\sum_{\lambda_i<0} I_i - \sum_{\lambda_i>0} I_i\right) \tag{3}$$

where I_i are the optical intensities corresponding to the eigenvalues λ_i of J.

The photonic hardware used is the SmartLight processor, a general-purpose platform comprising 17 hexagonal cells and 72 programmable unit cells (PUCs), see Fig. 2a. As illustrated in Fig. 2b, an input splitter tree first distributes laser power into multiple paths. An array of dual-drive MZIs

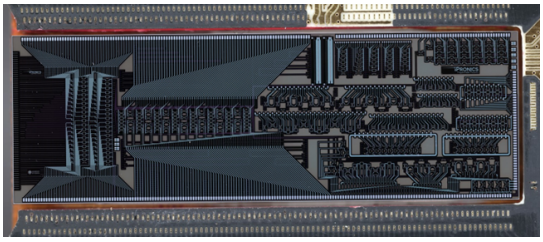

(a)

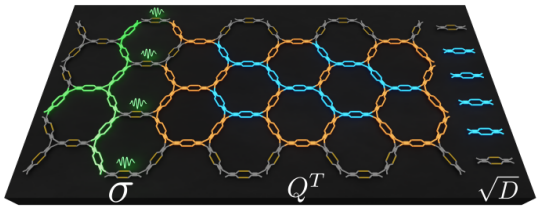

(b)

Fig. 2: (a) Image of the programmable photonic chip in the Smartlight processor and (b) Schematic represeantation of the hexagonal processor configured for Hamiltonian calculation. The green elements represent the splitter tree and the input encoding of the spin state, the blue an orange elements are configured to perform a 4x4 unitary transformation on the hexagonal mesh while the final array of blule elements implements the diaognal multiplication. The signals are photodetected with on-chip detection.

encodes each spin bit $\sigma_i = \pm 1$ into the amplitude and phase of the optical field: bar state sets the amplitude, while dual phase shifters introduce the ± 1 sign. A rectangular MZI network implements the orthogonal matrix Q following the Clements design [15], and a subsequent MZI stage encodes the diagonal matrix $\sqrt{D}$. Although the mesh is natively unitary, this ancillary stage enables non-unitary multiplications, the first such demonstration on a general-purpose photonic mesh. On-chip photodiodes then convert the output intensities into electrical signals proportional to $H(\sigma)$.

A digital controller completes the solver by executing a simulated-annealing loop. At each iteration, the measured energy determines whether to flip a randomly chosen spin according to a temperature-dependent acceptance probability. High temperatures allow broad exploration of the energy landscape, while gradual cooling ensures convergence to the ground state. The algorithm proceeds as shown in Algorithm 1

III. Experimental Results

A. Hamiltonian Calculation

The experimental validation of on-chip Hamiltonian computation proceeded in three stages. First, we generated 500 random coupling matrices of size 3×3 and 400 of size 4×4, and performed an eigendecomposition to obtain Q and $\sqrt{D}$. These matrices were loaded into the SmartLight processor, which implements Q via a rectangular MZI network with fidelities of $99.2 \pm 0.3\%$ for 3×3 and $98.4 \pm 0.3\%$ for 4×4

Algorithm 1 Simulated-Annealing Loop for Photonic Ising Solver

Require: Coupling matrix J, initial temperature T_0, cooling factor α, max iterations $N_{\max}$

Decompose $J = Q\,\Lambda\,Q^T$, factor $\Lambda = \sqrt{D}\,\sqrt{D}$
Program photonic mesh with Q and $\sqrt{D}$
Randomly initialize spin vector $\sigma^{(0)}$
for $n = 0$ to $N_{\max} - 1$ **do**
  Measure $H(\sigma^{(n)})$ via on-chip intensity readout
  Propose σ' by flipping one spin in $\sigma^{(n)}$
  Measure $H(\sigma')$
  $\Delta H \leftarrow H(\sigma') - H(\sigma^{(n)})$
  if $\Delta H \leq 0$ **then**
    $\sigma^{(n+1)} \leftarrow \sigma'$
  else
    Accept σ' with probability $\exp(-\Delta H/T_n)$; otherwise keep $\sigma^{(n)}$
  end if
  $T_{n+1} \leftarrow \alpha\,T_n$
end for

Ensure: Best configuration found (lowest H)

(bit precision $>$ 5bits) as shown in Fig. 3a. Next, diagonal entries were normalized to $[0, 1]$ by dividing by the maximum eigenvalue, and this factor, squared, was used to scale the photocurrents upon detection.

Second, all 2^3 (3×3) and 2^4 (4×4) spin configurations were encoded using an array of dual-drive MZIs: each MZI was set to the *bar* state to impose unit amplitude, while the sign of $\sigma_i = \pm1$ was realized by tuning both phase shifters. On-chip photodiodes then measured intensities $I_i = |(\sqrt{D}Q\sigma)_i|^2$, from which the Hamiltonian values were computed using Eq. (3), yielding 4000 and 6400 measurements for the two cases.

Finally, we compared these measured Hamiltonians against the theoretical values (Fig. 3b), obtaining coefficients of determination $r^2 = 0.99$ for the 3×3 case and $r^2 = 0.98$ for 4×4. The error distributions exhibit mean squared errors of 0.007 and 0.016, respectively, demonstrating high-accuracy Hamiltonian evaluation across all configurations.

B. 3-Node Problem

As a benchmark, we consider the canonical three-spin ferromagnetic lattice [16], in which each spin interacts with its two neighbors and experiences a small external bias $h = 0.01$. The coupling strengths satisfy $J_1 = J_2 = 1$, while J_3 is varied via the ratio

$$\alpha = \frac{J_3}{J_2},$$

swept from -1.5 to 1.5 in steps of 0.1. For each α, we experimentally performed 1000 independent simulated-annealing runs of 100 iterations each, and computed the success probability as the fraction of runs that converged to the ground-state configuration.

In Fig. 4a we present a representative energy trace alongside an inset of success probabilities across all configurations for α = 1.5. The success probability for all α values is presented in Fig. 4b. In most cases, the optimal state (highlighted in green) is reached with unity probability and within 40 iterations. Notable exceptions occur at $\alpha = -0.9$ and -1.0, where no runs found the ground state, and at $\alpha = -1.5$ and -1.3, which exhibit reduced success probabilities of 0.962 and 0.945, respectively.

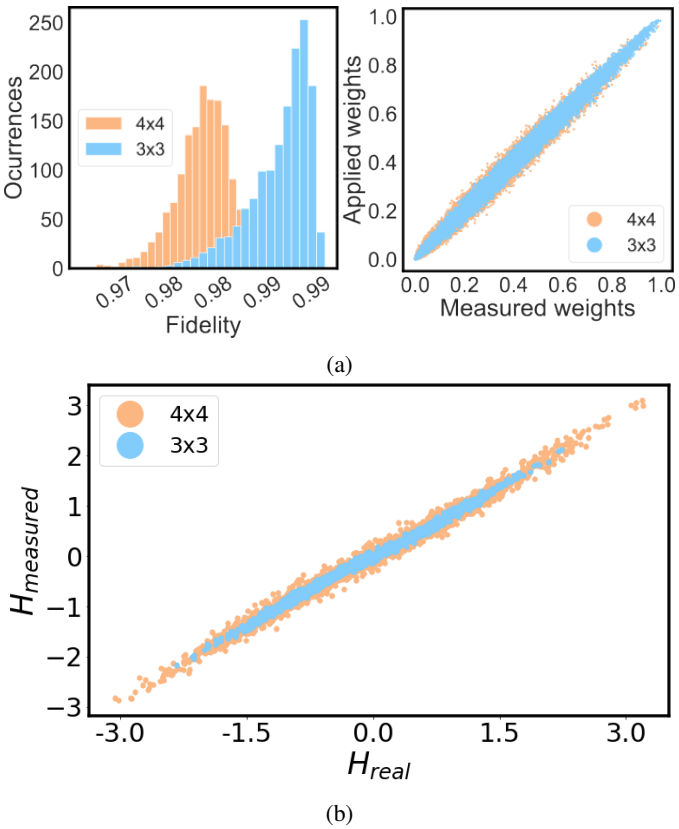

Fig. 3: (a) Experimental measured fidelity of 3x3 and 4x4 unitary matrices on the hexagonal processor and the comparison between the target and measured weights. (b) Comparison between the expected and measured hamiltonian for 400 3×3 and 500 4×4 coupling matrices, and all 2^3 (3×3) and 2^4 (4×4) spin configurations.

IV. Conclusions

We have presented the first on-chip programmable photonic Ising machine, implemented on a general-purpose hexagonal MZI mesh. Using the SmartLight processor, we first show the encoding of 3×3 and 4×4 unitary matrices obtaining fidelities of $99.2 \pm 0.3\%$ and $98.4 \pm 0.3\%$, respectively. Then, we performed 4000 3×3 and 6400 4×4 Hamiltonian evaluations with mean squared errors of 0.007 and 0.016, respectively. Coupled to a simulated-annealing feedback loop, the system solved the three-spin ferromagnetic benchmark across a wide range of coupling ratios, achieving unity success probabilities in under 40 iterations for most cases. These results validate the viability of reconfigurable photonic meshes

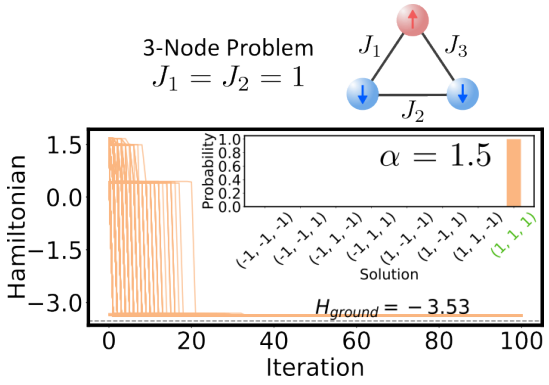

(a)

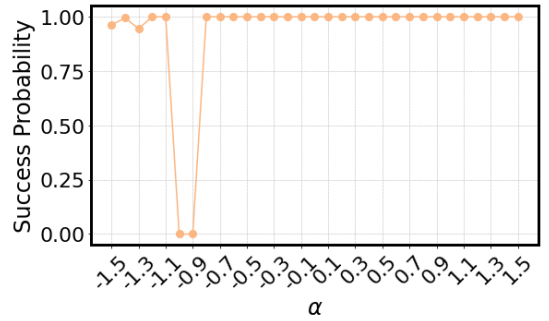

(b)

Fig. 4: (a) Evolution of the measured Hamiltonian during optimization of the three-node problem on the hexagonal processor for α = 1.5. H_{ground} denotes the Hamiltonian of the ground-state solution. Inset: success probability of each possible spin configuration. (b) Success probability as a function of α.

for combinatorial optimization and lay the groundwork for extending this architecture to larger problem instances.

References

[1] A. Lucas, "Ising formulations of many np problems," *Frontiers in physics*, vol. 2, p. 5, 2014.

[2] F. Glover and G. A. Kochenberger, *Handbook of metaheuristics*. Springer, 2003.

[3] M. M. Waldrop, "The chips are down for moore's law," *Nature*, vol. 530, no. 7589, pp. 144–147, 2016.

[4] C. L. Trinh, H. S. Kim, and J. Kim, "High performance computing and big data analytics: An overview," *Big Data Research*, vol. 22, p. 100 150, 2020.

[5] M. Yamaoka, C. Yoshimura, M. Hayashi, T. Okuyama, K. Aoki, and H. Mizuno, "20k-spin ising chip for combinational optimization problem with cmos annealing," in *IEEE International Solid-State Circuits Conference (ISSCC)*, 2015, pp. 1–3.

[6] S. Okuyama, K. Matsumoto, F. Matsukura, H. Ohno, *et al.*, "Magnetic tunnel junction based annealing computation for ising spin model," *Journal of Applied Physics*, vol. 117, no. 17, 17B717, 2015.

[7] T. Lanting, A. J. Przybysz, A. Y. Smirnov, *et al.*, "Entanglement in a quantum annealing processor," *Physical Review X*, vol. 4, no. 2, p. 021 041, 2014.

[8] R. Hamerly, T. Inagaki, P. L. McMahon, *et al.*, "Experimental investigation of performance differences between coherent ising machines and a quantum annealer," *Science advances*, vol. 5, no. 5, eaau0823, 2019.

[9] T. Inagaki, K. Inaba, R. Hamerly, K. Inoue, Y. Yamamoto, and H. Takesue, "Large-scale ising spin network based on degenerate optical parametric oscillators," *Nature Photonics*, vol. 10, no. 6, pp. 415–419, 2016.

[10] N. C. Harris, J. Carolan, D. Bunandar, *et al.*, "Large-scale quantum photonic circuits in silicon," *Nanophotonics*, vol. 5, no. 2, pp. 456–468, 2016.

[11] D. A. Miller, "Self-configuring universal linear optical component," *Photonics Research*, vol. 1, no. 1, pp. 1–15, 2013.

[12] J. Ouyang, Y. Liao, Z. Ma, *et al.*, "On-demand photonic Ising machine with simplified Hamiltonian calculation by phase encoding and intensity detection," *Communications Physics*, vol. 7, no. 1, p. 168, 2024, ISSN: 2399-3650. DOI: 10.1038/s42005-024-01658-x. [Online]. Available: https://doi.org/10.1038/s42005-024-01658-x.

[13] S. Kirkpatrick, C. D. Gelatt, and M. P. Vecchi, "Optimization by simulated annealing," *Science*, vol. 220, no. 4598, pp. 671–680, 1983.

[14] D. Pérez-López, A. Gutierrez, D. Sánchez, *et al.*, "General-purpose programmable photonic processor for advanced radiofrequency applications," *Nature Communications 2024 15:1*, vol. 15, no. 1, pp. 1–11, Feb. 2024, ISSN: 2041-1723. DOI: 10.1038/s41467-024-45888-7. [Online]. Available: https://www.nature.com/articles/s41467-024-45888-7.

[15] W. R. Clements, P. C. Humphreys, B. J. Metcalf, W. S. Kolthammer, and I. A. Walmsley, "Optimal design for universal multiport interferometers," *Optica*, vol. 3, no. 12, pp. 1460–1465, 2016. DOI: 10.1364/OPTICA.3.001460. [Online]. Available: http://www.osapublishing.org/optica/abstract.cfm?URI=optica-3-12-1460.

[16] S. Y. Kim, "Ising antiferromagnet on a finite triangular lattice with free boundary conditions," *Journal of the Korean Physical Society*, vol. 67, no. 9, pp. 1517–1523, Nov. 2015, ISSN: 19768524. DOI: 10.3938/JKPS.67.1517/METRICS. [Online]. Available: https://link.springer.com/article/10.3938/jkps.67.1517.